Sensors & Diagnostics

PAPER

Check for updates

Preparation and H$_2$S gas-sensitive properties of hierarchical flower-like Ag/ZnO composites

Dan Zhao, [iD] *[a] Liyue Song,[b] Xiaojing Bai,*[a] Haixiang Song,[a] Miaomiao Li,[a] Lijun Wang, [iD] [a] Baosheng Li,[c] Mingrui Yang,[b] Qiuyu Chen[d] and Lili Sui*[b]

In this research, a hierarchically structured, flower-like ZnO material was successfully synthesized *via* a solvothermal approach. Subsequently, silver (Ag) nanoparticles were deposited onto the ZnO flowers through ultraviolet light reduction, yielding a highly efficient Ag/ZnO composite material. Notably, the 3 at% Ag/ZnO composite demonstrated a remarkably enhanced response to 100 ppm H$_2$S at a relatively low operating temperature of 92 °C, reaching 430.0, which is significantly higher than the 157.3 observed for the pristine ZnO material. Furthermore, the detection limit for H$_2$S was dramatically lowered from 0.05 ppm to a mere 1 ppb. The findings of this research suggest that the incorporation of Ag nanoparticles substantially ameliorates the H$_2$S sensing capabilities of the pure ZnO material. To delve deeper into the underlying mechanisms, X-ray photoelectron spectroscopy (XPS) was utilized to explore the interaction between the Ag/ZnO sensor and H$_2$S gas. This analysis provided valuable insights into the reasons behind the observed enhancement in gas sensing performance, shedding light on the synergistic effects of the Ag nanoparticles and the ZnO matrix in the composite material.

1. Introduction

The pace of modern scientific and industrial progress has been remarkable, driven by the ever-growing needs of human society. Yet, this swift advancement has not come without its drawbacks, such as environmental pollution, which poses a significant challenge to the human living environment. The insidious effects of vehicular emissions, unregulated industrial discharges, and the release of noxious gases during home renovations are all significant threats to both the environment and human health. In light of these concerns, accurate and real-time monitoring of toxic and harmful gases has become increasingly important. Hydrogen sulfide (H$_2$S), a colorless gas with an acrid odor, is particularly hazardous. It can cause a range of adverse health effects, from dizziness and nausea to respiratory distress and, in extreme cases, can be fatal. Prolonged exposure can lead to severe irritation and damage to the eyes, skin, and respiratory system. Given the risks associated with H$_2$S, the development of high-performance gas sensors is of paramount importance. These sensors can significantly enhance our capacity to gather, process, and analyze data, thereby improving the precision of real-time hazard prediction and reducing the incidence of accidents. While existing detection methods like infrared spectroscopy,[1] gas chromatography,[2] and spectrometry[3] offer high accuracy and stability, they are often characterized by high costs, large size, and limited portability. These factors restrict their use primarily in laboratory settings, hindering their widespread adoption in everyday applications. In response to this challenge, a compact, cost-effective, easy to operate, and practical gas sensor has emerged, making it an ideal choice for practical, easy-to-use monitoring solutions.[4–10] These advancements hold the promise of a safer and more secure environment for all.

Recently, gas sensors based on semiconductor metal oxide have been the focus in the gas sensor area. The creation of intricate or multi-tiered nanostructures has emerged as a dependable approach to augmenting their sensing capabilities. Such hierarchical structures, crafted from low-dimensional elements, boast a three-dimensional configuration that minimizes particle agglomeration. This design facilitates the efficient adsorption of gas molecules on the sensor's surface and expedites electron transfer, thereby significantly enhancing the sensor's gas detection prowess.[11,12] In the current landscape, various ZnO materials with hierarchical structures are prepared; they are mainly constructed from simple nanoparticles, nanosheets, nanowires, *etc.* into hollow tubular,

[a] Henan Province International Joint Laboratory of Nanocomposite Sensing Materials, Anyang Institute of Technology, Anyang, Henan, 455000 China. E-mail: baixiaojing@ayit.edu.cn
[b] Qiqihar University, Qiqihar 161000, China. E-mail: sui_leelee@126.com
[c] Henan Province of Key Laboratory of New Opto-electronic Functional Materials, College of Chemistry and Chemical Engineering, Anyang Normal University, Anyang, Henan, 455000, China
[d] Qiqihar Environmental Monitoring Station, Qiqihar 161000, China

array-like, hollow spherical, flower-like structures. The fabrication techniques employed are diverse and include hydrothermal/solvothermal methods,[13] microwave-assisted hydrothermal synthesis,[14] template-assisted methods,[15] chemical vapor deposition,[16] and thermal evaporation.[17] For instance, Qu et al.[18] successfully developed a three-dimensional sea urchin-like ZnO micro-/nanosphere array sensor using a one-step thermal evaporation technique. This sensor demonstrated a robust response of 15.0 to 200 ppm ethanol at an optimal operating temperature of 280 °C, with swift response and recovery times of 4 s and 14 s, respectively. Similarly, Han et al.[19] utilized polystyrene spheres (PSS) as a template to fabricate highly crystalline ZnO hollow spheres through a hydrothermal process. At a comparatively higher operating temperature of 385 °C, these sensors exhibited a response of 57.6 to 100 ppm n-butanol, with response and recovery times of 36 s and 9 s, and a detection limit of 10 ppm. Despite these advances, hierarchical ZnO materials in the domain of gas sensing still grapple with challenges such as the requirement for high operating temperatures and the pursuit of greater sensitivity, indicating a need for further innovation and optimization in sensor technology.

Noble metals, endowed with substantial work functions and exceptional catalytic prowess, have proven to be exemplary dopants in the enhancement of metal oxide-based gas sensing devices. Their integration not only diminishes the activation energy required for the chemical adsorption of gases but also endows sensors with the ability to selectively detect specific gases.[20] The incorporation of silver into zinc oxide's hierarchical structures has opened up promising horizons in optoelectronics and sensor technology. Shen et al.[21] employed precipitation to decorate the surface of 3D porous ZnO microspheres with Ag nanoparticles, resulting in a TEA gas sensor of remarkable sensitivity and swift response. This sensor demonstrated a response of 6043 to 100 ppm TEA, an impressive 14.8-fold increase over that of a pure ZnO sensor. Moreover, the optimal operating temperature for this sensor was notably reduced from 230 °C to a more manageable 183.5 °C. The sensor also boasts expedited response and recovery times, with a detection limit reduced from 1 ppm to an even more sensitive 0.5 ppm. Yousefi et al.[22] leveraged the sol–gel method to fabricate Ag-doped ZnO nanoparticles. Gas sensitivity tests revealed that a sensor optimized with 3.5 wt% Ag displayed superior selectivity for ethanol over its pure ZnO counterpart. Given the catalytic attributes of noble metals and their capacity to significantly amplify the material's surface area, doping with such metals stands out as an efficacious strategy for bolstering the gas-sensing capabilities of materials. In light of these considerations, the present study will delve into the use of ultraviolet (UV) reduction to deposit Ag particles onto flower-like ZnO structures. The ensuing investigation into the gas sensing performance of the Ag/ZnO composite materials is poised to make a substantial contribution to the advancement of optoelectronic device performance, the enhancement of sensor sensitivity, and the broadening of their industrial and scientific applications. Furthermore, this research endeavors to

provide new ideas and development directions for the utilization of Ag/ZnO in the burgeoning domain of gas sensor technology.

2. Experimental section

2.1. Preparation of hierarchical flower-like Ag/ZnO composites

All reagents are of analytical grade and were used without further purification. The preparation of hierarchical flower-like ZnO[23] is detailed in the SI. Preparation of hierarchical flower-like Ag/ZnO: 0.05 g of the prepared ZnO sample was added to 3.7 mL of silver nitrate solution with a concentration of 0.005 mol L^{-1}, and then ethanol was added to maintain the total volume of the solution at 30 mL. The solution was irradiated with ultraviolet light for 30 minutes, during which it changed from white to gray. After that, a gray precipitate was obtained after washing three times with deionized water and ethanol and by centrifugation, followed by drying at 70 °C for 8 h and calcination at 300 °C in air for 1 h, resulting in 3 at% Ag/ZnO nanocomposite material. The basic characterization of the material and the preparation and test parameters of the sensor[24,25] are detailed in the SI.

3. Results and discussion

3.1. Structure and morphology

The phase of Ag/ZnO samples with different Ag-loaded molar ratios was determined by XRD analysis on Ag/ZnO, as shown in Fig. 1. Diffraction peaks appear at 31.7°, 34.3°, 36.2°, 47.4°, 56.5°, 62.7°, 66.3°, 67.8°, 69.0°, 72.4°, and 76.8° corresponding to the (100), (002), (101), (102), (110), (100), (200), (112), (201), (004) and (202) crystal planes of ZnO (JCPDS card no.79-0208). When the loading of Ag is less than 1 at%, there is no characteristic peak of Ag, which may be due to the small
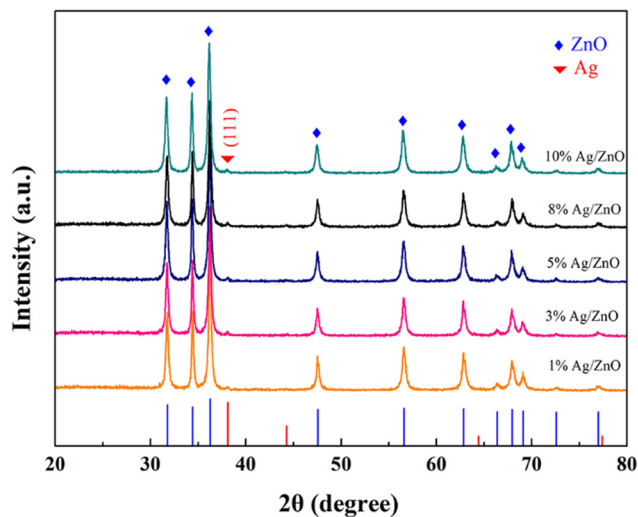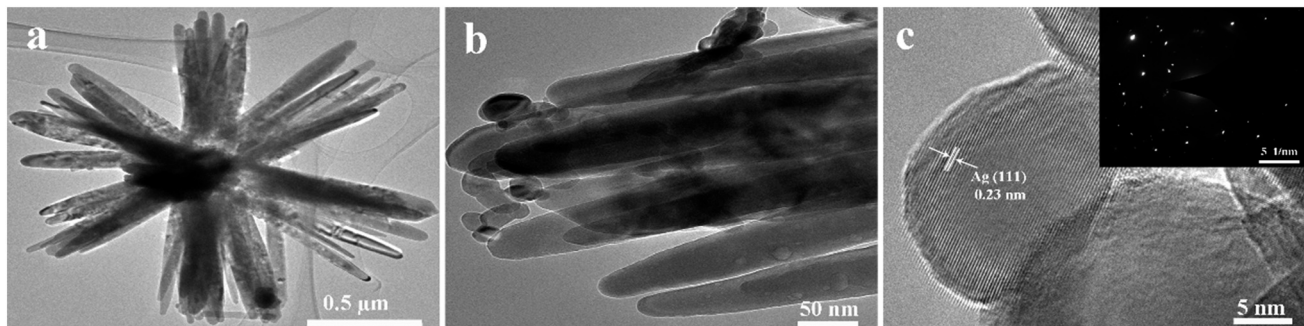

Fig. 1 XRD patterns of Ag/ZnO loaded with different Ag molar ratios (1 at%, 3 at%, 5 at%, 8 at%, 10 at%).

Table 1 The ICP detection results of flower-like Ag/ZnO with Ag/Zn mole ratios of 1 at%, 3 at%, 5 at%, 8 at% and 10 at%

Flower-like Ag/ZnO	1#	2#	3#	4#	5#
• Theoretical molar ratio of Ag/Zn (at%)	1	3	5	8	10
Molar ratio of Ag/ZnO measured by ICP (at%)	0.6	2.1	4.5	7.4	9.2

Fig. 2 (a and b) TEM and (c) HRTEM (inset of c) SAED images of Ag/ZnO composites with a molar ratio of 3 at% Ag.

amount of Ag loading. With the increase of Ag amount, the (111) crystal plane diffraction peak belonging to Ag can be seen at 38.1° (JCPDS no. 87-0597), and the peak gradually becomes stronger with the increase of Ag loading, indicating that the obtained product is Ag/ZnO composite. Compared with pure ZnO, the diffraction peaks of ZnO in all Ag/ZnO materials are not shifted, so Ag is located on the surface of ZnO and is not incorporated into its crystal lattice.
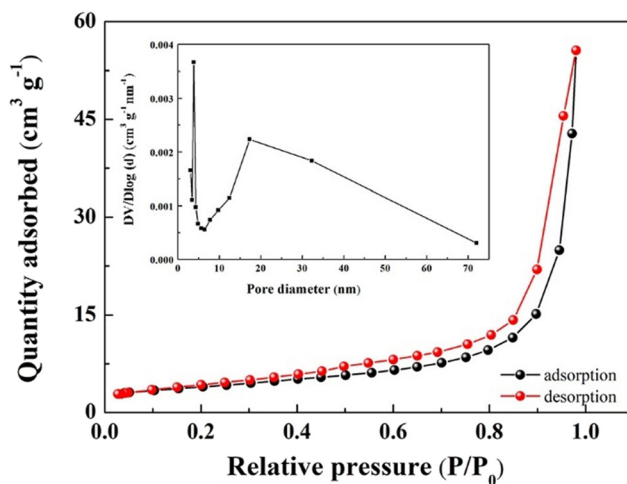
In order to further determine the actual composite molar ratio of Ag in flower-like Ag/ZnO, inductively coupled plasma (ICP) technology was used to determine the flower-like Ag/ZnO materials with different Ag/Zn molar ratios, and the data are shown in Table 1. The results show that Ag is present in these products, and the actual loading Ag/Zn molar ratio is lower than the theoretically calculated Ag/Zn molar ratio, which may be due to a certain loss in the process of ultraviolet light reduction deposition.

The fine structure of Ag/ZnO and the loading of Ag on flower-like ZnO were further determined by TEM and HRTEM. Fig. 2a shows the structure of flower-like Ag/ZnO with an Ag molar ratio of 3 at%. Ag nanoparticles are irregularly distributed on the surface of the ZnO flower-like structure with a particle size of 15–30 nm (Fig. 2b). The HRTEM plot (Fig. 2c) shows a regular lattice fringe distribution with a lattice spacing of 0.23 nm for the nanoparticles, matching the (111) plane of silver element (SI Fig. S1). The above results further confirmed that the synthesized product was an Ag/ZnO composite. The corresponding SAED plot (inset in Fig. 2c) reveals the single-crystal characteristics of the Ag/ZnO flowers.

The N_2 adsorption–desorption and pore size distribution curves of the Ag/ZnO composites with a molar ratio of 3 at% are shown in Fig. 3, from which it can be seen that the nitrogen adsorption–desorption curves of the materials belong to type IV isotherms with H3 hysteresis rings, and the specific surface area of the composites is calculated to be

20.572 $m^2 g^{-1}$. The BJH distribution map (inset) shows that the main pore sizes are 3.8 nm and 17 nm, which confirms the mesoporous properties of Ag/ZnO. After Ag particles are loaded, the specific surface area of the material is larger than that of the pure phase ZnO material. The reason for the increase in specific surface area might be attributed to the synergistic effect resulting from the morphological regulation caused by the Ag nanoparticles and the inhibition of the agglomeration of ZnO particles; the larger specific surface area is more conducive to the improvement of the gas sensitivity of the material.

The elemental and valence states of 3 at% Ag/ZnO were analyzed by XPS. From the full spectrum (Fig. 4a), it can be seen that except for the standard C peak, the obtained material consists of only Zn, Ag and O elements, indicating

Fig. 3 N_2 adsorption–desorption curve and pore size distribution (inset) of Ag/ZnO composites with a molar ratio of 3 at% Ag.
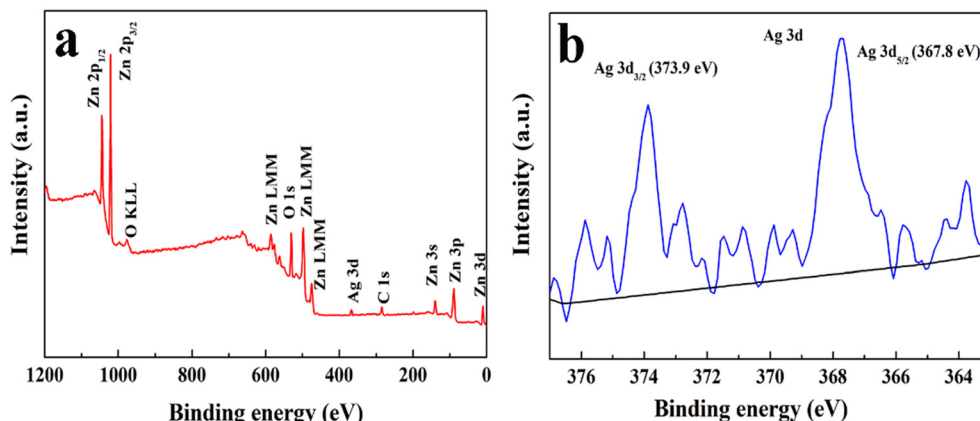
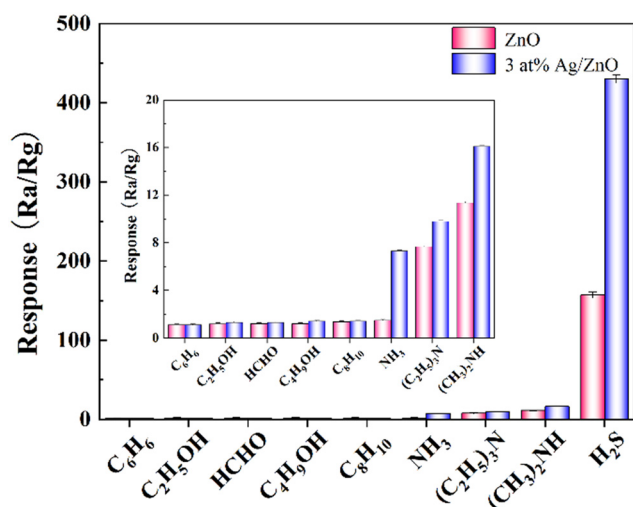Fig. 4 The XPS spectra of Ag/ZnO composites with a molar ratio of 3 at% Ag: (a) full survey, (b) Ag 3d.

Fig. 5 Responses of 3 at% Ag/ZnO sensor to 100 ppm of different gases at 92 °C.

temperature increases, the response initially increases and then decreases, and reaches its maximum response of 100 ppm of H_2S at 92 °C. Therefore, the optimal operating temperature is determined to be 92 °C (SI Fig. S2). Selectivity is an important parameter to evaluate whether the sensor can accurately determine the target gas in the actual complex environment. Fig. 5 shows the response of a 3 at% Ag/ZnO sensor to 100 ppm H_2S and eight other interfering gases at an operating temperature of 92 °C. The response data of Ag/ZnO gas sensing element to benzene (C_6H_6), ethanol (C_2H_5OH), formaldehyde (HCHO), n-butanol (C_4H_9OH), xylene (C_8H_{10}), ammonia (NH_3), triethylamine ((C_2H_5)$_3$N), dimethylamine ((CH_3)$_2$NH) and hydrogen sulfide (H_2S) are shown in Table 2, and the selectivity coefficients ($K_{H2S/X}$) of H_2S gas for the other eight gases are 390.9, 330.8, 330.8, 307.1, 307.1, 58.9, 43.9, and 26.7, respectively, indicating that the 3 at% Ag/ZnO sensor has good selectivity for H_2S gases. In addition, the 3 at% Ag/ZnO sensor showed a higher response for these nine gases than the pure ZnO sensor, which proved that the Ag load could effectively improve the gas sensing performance of the ZnO gas sensor for H_2S.

The response recovery curves of the 3 at% Ag/ZnO sensor to different concentrations of H_2S gas at an optimal operating temperature of 92 °C are shown in Fig. 6. Fig. 6a and b show the response and recovery time of the 3 at% Ag/ZnO composites to H_2S at concentrations of 1–100 ppm and 1–100 ppb at 92 °C, respectively; the specific data are shown in Table 3. The response and recovery time of the composites to 100 ppm H_2S are 18.2 s and 6012 s, respectively, which is longer than that of pure phase ZnO (3 s) and shorter than recovery time (6399 s). The increase in response time can be attributed to the increase of 3 at% Ag ZnO. The response of the ZnO sensor to H_2S increases. In

that Ag is successfully loaded on ZnO. Fig. 4b shows the fine spectrum of Ag 3d, with the peaks at 367.8 eV and 373.9 eV corresponding to Ag $3d_{5/2}$ and Ag $3d_{3/2}$, respectively, which are split by Ag 3d, indicating that Ag exists as elemental Ag.[26]

3.2. Gas-sensitive properties of hierarchical structure flower-like Ag/ZnO

Due to the significant influence of the operating temperature on the sensitivity performance of the gas sensor, as the operating

Table 2 The response results of 3 at% Ag/ZnO sensor and ZnO sensor to 100 ppm of nine gases at 92 °C

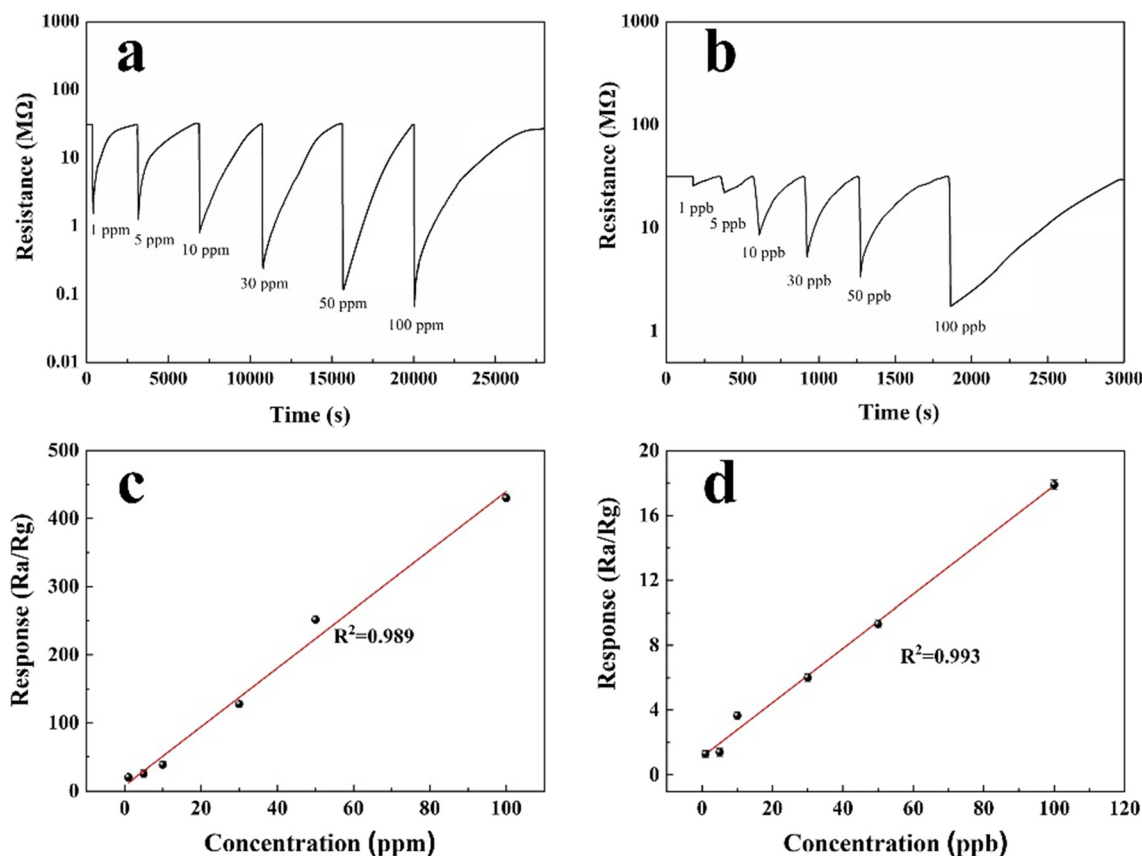| Test gases (100 ppm)	Benzene	Ethanol	Formaldehyde	n-Butanol	Xylene	NH_3	Triethylamine	Dimethylamine	H_2S
ZnO	1.1	1.2	1.2	1.3	1.3	1.4	7.7	11.4	157.3
3 at% Ag/ZnO	1.1	1.3	1.3	1.4	1.4	7.3	9.8	16.1	430.0

Fig. 6 Ag/ZnO sensor with 3 at% Ag load molar ratio at 92 °C: (a) response recovery curve and (c) linear relationship for 1–100 ppm H_2S gas, (b) response recovery curve and (d) linear relationship for 1–100 ppb H_2S gas.

addition, the response of the corresponding Ag/ZnO gas sensor to 1–100 ppm and 1–100 ppb H_2S is shown in Fig. 6c and d. With the increase of H_2S gas concentration, the gas response increases accordingly, and there is a good linear relationship between the concentration of 1–100 ppm and 1–100 ppb; the correlation coefficients are $R^2 = 0.989$ and $R^2 = 0.993$, respectively. The minimum detection limit for the 3 at% Ag/ZnO sensor is 1 ppb (response is 1.4). In summary, compared with the pure phase ZnO material, the response of the 3 at% Ag/ZnO sensor to 100 ppm H_2S

increased from 157.3 to 430.0 in the pure phase and the minimum detection limit decreased from 0.05 ppm to 1 ppb at the same operating temperature of 92 °C.

In order to evaluate the feasibility of the gas sensor in practical applications, the moisture resistance and long-term stability of the gas sensor were tested. As shown in Fig. 7a, the response of the Ag/ZnO sensor in the range of 11.3–93.6% relative humidity (RH) is less than 1.3 at 92 °C, indicating that the influence of ambient humidity on H_2S gas is negligible when the Ag/ZnO sensor measures H_2S gas at 92

Table 3 The responses, response and recovery times of 3 at% Ag/ZnO to different concentrations of H_2S at 92 °C

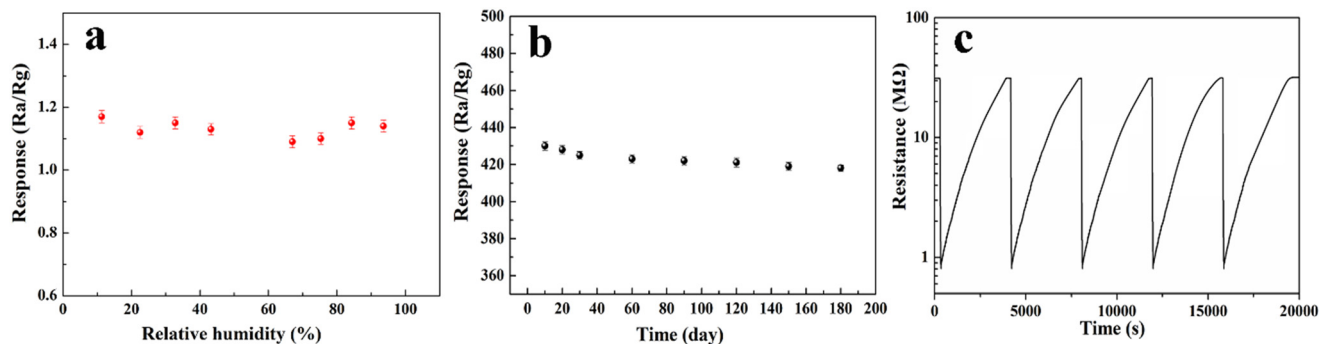| Gas concentration	Response (s)	Response time (s)	Recovery time (s)
1 ppb	1.3	58.5	120
5 ppb	1.4	50.2	141
10 ppb	3.6	42.2	270
30 ppb	6.0	21.4	324
50 ppb	9.3	14.9	553
100 ppb	17.9	53.4	1057
1 ppm	20.1	52.6	2642
5 ppm	25.1	54.2	3666
10 ppm	38.5	40.4	3755
30 ppm	127.7	40	3536
50 ppm	251.5	32.2	4283
100 ppm	430.0	18.2	6012

Fig. 7 Response of the 3 at% Ag/ZnO sensor at 92 °C: (a) the responses in different relative humidity atmosphere, (b) long-term stability to H₂S, (c) repeatability to 10 ppm H₂S.

°C. Fig. 7b is a recording of the sensor's response every 10 days after the first test of 100 ppm H_2S over 180 days to explore its long-term stability. The results show that the standard error change of the sensor is less than 5% within 180 days, indicating that the sensor has good long-term stability. The Ag/ZnO sensor also showed excellent reproducibility in the H_2S test (Fig. 7c), with the Ag/ZnO sensor response for five consecutive tests of 10 ppm H_2S being 38.5, 38.3, 38.4, 38.5, and 38.5, respectively, with a standard deviation of 0.09.

3.3. Mechanism of hierarchical structure flower-like Ag/ZnO sensitivity to H₂S

XPS technology was used to analyze the elemental changes of the 3 at% Ag/ZnO sensor before and after exposure to H_2S.

Fig. 8 shows the fine spectra of Zn 2p, O 1s and S 2p before and after contact with H_2S. Fig. 8a and d show the Zn 2p spectra before and after exposure to H_2S, respectively. As can be seen from the figure, the binding energy peaks of 1021.7/1021.6 eV and 1044.7/1044.6 eV before and after exposure to H_2S correspond to Zn 2p3/2 and Zn 2p1/2, respectively, indicating that Zn in 3 at% Ag/ZnO always exists at +2 valence.[27] The spin–orbit splitting value of Zn 2p between Zn 2p3/2 and Zn 2p1/2 is about 23 eV, which is consistent with the value of pure ZnO, indicating that Ag loading has no effect on Zn 2p.

As can be seen from the fine spectra of O 1s before and after contact with H_2S (shown in Fig. 8b and e), the three peaks of O 1s are located at 530.5/530.4 eV, 531.6/531.5 eV, and 532.6/532.4 eV, corresponding to lattice oxygen, chemisorption oxygen, and hydroxyl oxygen, respectively.
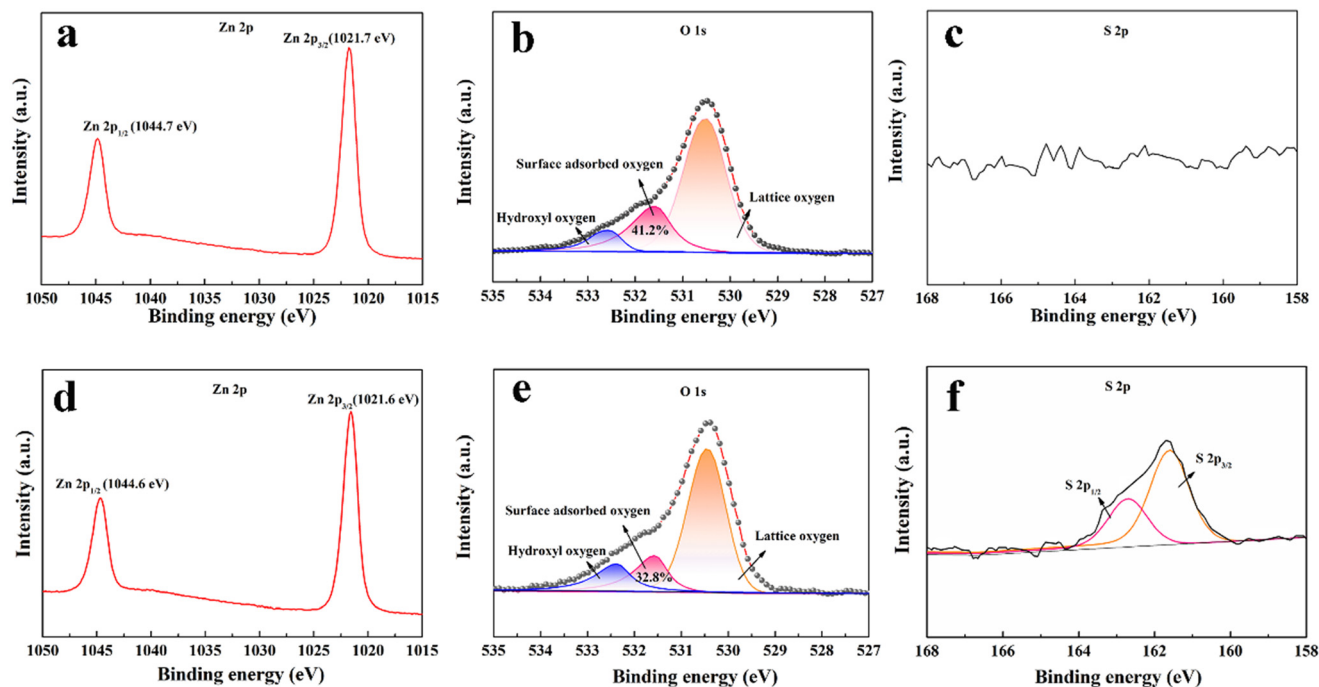

Fig. 8 The XPS spectra of Zn 2p, Ag 3d and O 1s of 3 at% Ag/ZnO composites (a–c) before and (d–f) after exposure to H₂S gas at 92 °C.
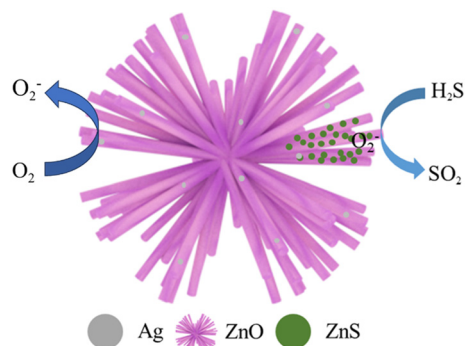
Fig. 9 Schematic diagram of the sensitivity mechanism of the Ag/ZnO sensor to H_2S gas at 92 °C.

Compared with the pure-phase ZnO, the chemisorption oxygen content of 3 at% Ag/ZnO increased from 39.8% to 41.2% of the pure-phase ZnO, and the increase in the adsorbed oxygen content played a key role in improving the sensing performance.[28] It is worth noting that the content of adsorbed oxygen on the surface of Ag/ZnO decreased from 41.2% to 32.8% after exposure to H_2S, indicating that the surface-adsorbed oxygen reacted with H_2S in a redox reaction. Fig. 8c shows that there is no obvious characteristic peak of S 2p in the material before contact with H_2S, indicating that there is no S element in the material before contact with H_2S. Fig. 8f shows the XPS fine spectra of S 2p after Ag/ZnO exposure to H_2S, and the peaks at 161.6 and 162.7 eV correspond to S^{2-} in the Zn–S bond.

In summary, when the Ag/ZnO gas sensing element is exposed to the reducing gas H_2S at 92 °C, its gas sensing mechanism is similar to that of pure phase ZnO to H_2S; that is, the surface-adsorbed oxygen (O_2^-) on Ag/ZnO reacts with H_2S to produce SO_2 and H_2O (eqn (1)), and at the same time, H_2S also interacts with ZnO to form ZnS (eqn (2)), and the reaction mechanism diagram is shown in Fig. 9.
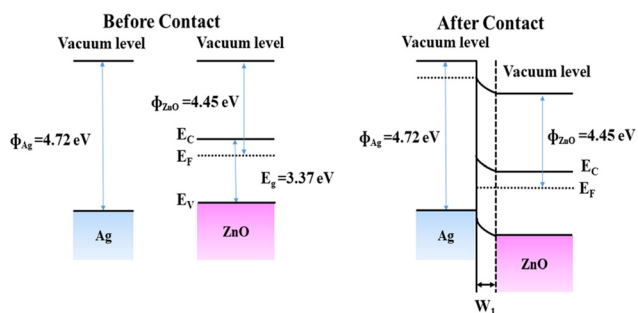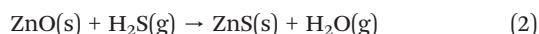
$$2H_2S(ads) + 3O_2^-(ads) \rightarrow 2SO_2(g) + 2H_2O(g) + 3e^- \quad (1)$$

$$ZnO(s) + H_2S(g) \rightarrow ZnS(s) + H_2O(g) \quad (2)$$

When Ag nanoparticles are introduced into ZnO materials, more active sites and the dissociation of oxygen molecules are promoted, and more oxygen molecules can be transferred from Ag nanoparticles to the surface of ZnO, which promotes the gas-sensitive reaction and improves the gas-sensitive performance.

In addition, the work functions of Ag and ZnO are 4.26 and 4.45 eV, respectively,[29] and the Fermi level of ZnO is higher than that of Ag due to its electron sensitization effect. When ZnO combines with Ag, electrons will transfer from ZnO to Ag until the Fermi level is in equilibrium, as shown in Fig. 10. The contact region forms an additional electron depletion layer, which increases the initial resistance and improves the gas sensing performance of Ag/ZnO. In addition, the ZnS generated by the interaction between ZnO and H_2S can increase the conductivity and surface active sites of the sensor, resulting in better gas sensing performance.

Conclusion

In this paper, flower-like ZnO materials with hierarchical structures were successfully prepared by dissolving heat method without adding any surfactant or template, and Ag/ZnO sensors with different loads were prepared by ultraviolet light reduction. The 3 at% Ag/ZnO sensor had a response of 430.0 to 100 ppm H_2S at 92 °C, a response time of 18.2 s and a recovery time of 6012 s, and a detection limit of 1 ppb. Compared with the pure phase ZnO sensor, the 3 at% Ag/ZnO sensor has a significantly higher response to 100 ppm H_2S, a lower detection limit, and a reduced recovery time. The strategic loading of an optimal quantity of Ag particles serves to augment the material's specific surface area, thereby enhancing its interaction with the target gas. This enhancement is attributed to a dual sensitization mechanism: chemical sensitization, which modulates the chemical interactions at the sensor's surface, and electron sensitization, which influences the electronic properties of the material. Collectively, these effects culminate in an improved gas sensing performance, underscoring the efficacy of the Ag/ZnO composite in detecting H_2S gas.

Conflicts of interest

The authors declare no competing financial interest.

Data availability

All data generated during this study are included in the manuscript and its supplementary information (SI) files. The datasets generated and analyzed during the current study are available from the corresponding author on reasonable request. Supplementary information is available. See DOI: https://doi.org/10.1039/d5sd00105f.

Acknowledgements

Fig. 10 Energy band levels of Ag and ZnO (a) before contact and (b) after contact.

References

1 Z. Y. Wu, Y. H. Gong and Q. X. Yu, Photoacoustic spectroscopy detection and extraction of discharge feature gases in transformer oil based on 1.5μ tunable fiber laser, *Infrared Phys. Technol.*, 2013, **58**, 86–90, DOI: 10.1016/j.infrared.2013.01.002.

2 N. Maksymovych, O. Ripko, O. Maksymovych, O. Kaskevych, N. Nikitina, V. Ruchko, O. Kuzko and V. Yatsimirsky, Adsorption semiconductor detector for malfunction diagnosis of high voltage transformers, *Sens. Actuators, B*, 2003, **93**, 321–326, DOI: 10.1016/s0925-4005(03)00217-x.

3 C. L. Wang, A. Liu, X. L. Yang, J. Wang, R. You, Z. J. Yang and J. M. He, YSZ-based mixed-potential type highly sensitive acetylene sensor based on porous SnO_2/Zn_2SnO_4 as sensing electrode, *Sens. Actuators, B*, 2019, **293**, 116–172, DOI: 10.1016/j.snb.2019.05.006.

4 N. Yamazoe, G. Sakai and K. Shimanoe, Oxide semiconductor gas sensors, *Catal. Surv. Asia*, 2003, 7, 63–75, DOI: 10.1023/A:1023436725457.

5 K. W. Kao, M. C. Hsu, Y. H. Chang, S. Gwo and J. A. Yeh, A sub-ppm acetone gas sensor for diabetes detection using 10 nm thick ultrathin InN FETs, *Sensors*, 2012, **12**, 7157–7168, DOI: 10.3390/s120607157.

6 J. Kong, N. R. Franklin and C. W. Zhou, Nanotube molecular wires as chemical sensors, *Science*, 2000, **287**, 622–625, DOI: 10.1126/science.287.5453.622.

7 J. S. Furter and P. C. Hauser, Interactive control of purpose built analytical instruments with forth on microcontrollers a turial, *Anal. Chim. Acta*, 2019, **1058**, 18–28, DOI: 10.1016/j.aca.2018.10.071.

8 Q. Wan, Q. H. Li, Y. J. Chen, T. H. Wang, X. L. He, J. P. Li and C. L. Lin, Fabrication and ethanol sensing characteristics of ZnO nanowire gas sensors, *Appl. Phys. Lett.*, 2004, **84**, 3654–3656, DOI: 10.1063/1.1738932.

9 L. E. Kreno, K. Leong, O. K. Farha, M. Allendorf, R. P. V. Duyne and J. T. Hupp, Metal-Organic framework materials as chemical sensors, *Chem. Rev.*, 2012, **112**, 1105–1125, DOI: 10.1021/cr200324t.

10 F. Schedin, A. K. Geim, S. V. Morozov, E. W. Hill, P. Blake, M. I. Katsnelson and K. S. Novoselov, Detection of individual gas molecules adsorbed on graphene, *Nat. Mater.*, 2007, **6**, 652–655, DOI: 10.1038/nmat1967.

11 X. Sun, C. Wang, D. Su, G. X. Wang and Y. H. Zhong, Application of photocatalytic materials in Sensors, *Adv. Mater. Technol.*, 2020, **5**, 1900993, DOI: 10.1002/admt.201900993.

12 A. Moumen, G. C. W. Kumarage and E. Comini, P-type metal oxide semiconductor thin films: synthesis and chemical sensor applications, *Sensors*, 2022, **22**, 1359–1404, DOI: 10.3390/s22041359.

13 Q. Zhou, W. Chen, J. Li, C. Tang and H. Zhang, Nanosheet-assembled flower-like SnO_2 hierarchical structures with enhanced gas-sensing performance, *Mater. Lett.*, 2015, **161**, 499–502, DOI: 10.1016/j.matlet.2015.09.010.

14 S. H. Ferreira, M. Morais and D. Nunes, High uv and sunlight photocatalytic performance of porous ZnO nanostructures synthesized by a facile and fast microwave hydrothermal method, *Materials*, 2021, **14**, 2385–2402, DOI: 10.3390/ma14092385.

15 X. W. Lou, L. A. Archer and Z. Yang, Hollow micro−/nanostructures: synthesis and applications, *Adv. Mater.*, 2008, **20**, 3987–4019, DOI: 10.1002/adma.200800854.

16 H. H. Wang and C. S. Xie, Controlled fabrication of nanostructured ZnO particles and porous thin films via a modified chemical bath deposition method, *J. Cryst. Growth*, 2006, **291**, 187–195, DOI: 10.1016/j.jcrysgro.2006.02.043.

17 C. Xu, G. Xu, Y. Liu and G. H. Wang, A simple and novel route for the preparation of ZnO nanorods, *Solid State Commun.*, 2002, **122**, 175–179, DOI: 10.1016/s0038-1098(02)00114-x.

18 Y. W. Qu, Z. C. Song and J. Zhang, Enhanced gas-sensing to low-concentration ethanol gas from 3-dimensional (3D) urchin-like ZnO micro/nanospheres, *Mater. Lett.*, 2023, **335**, 133817–133820, DOI: 10.1016/j.matlet.2023.133817.

19 B. Q. Han, X. Liu, X. X. Xing, N. Chen, X. C. Xiao, S. Y. Liu and Y. D. Wang, A high response butanol gas sensor based on ZnO hollow spheres, *Sens. Actuators, B*, 2016, **237**, 423–430, DOI: 10.1016/j.snb.2016.06.117.

20 C. N. Wang, Y. L. Li and F. L. Gong, Yong-Hui Zhang, Shao-Ming Fang, Hao-Li Zhang, Advances in doped ZnO nanostructures for gas sensor, *Chem. Rec.*, 2020, **20**, 1553–1567, DOI: 10.1002/tcr.202000088.

21 Z. Shen, X. D. Zhang and R. N. Mi, Man Liu, Yu Chen, Chuan Chen, Shengping Ruan, On the high response towards TEA of gas sensors based on Ag-loaded 3D porous ZnO microspheres, *Sens. Actuators, B*, 2018, **270**, 492–499, DOI: 10.1016/j.snb.2018.05.034.

22 H. R. Yousefi, B. Hashemi, A. Mirzaei, H. Roshan and M. H. Sheikhi, Effect of Ag on the ZnO nanoparticles properties as an ethanol vapor sensor, *Mater. Sci. Semicond. Process.*, 2020, **117**, 105172–105181, DOI: 10.1016/j.mssp.2020.105172.

23 W. Z. Zhang, L. Y. Song and D. Zhao, Construction of hierarchical ZnO flower-like structure for boost H_2S detection at low temperature, *Sens. Actuators, B*, 2023, **385**, 133728, DOI: 10.1016/j.snb.2023.133728.

24 D. Zhao, X. F. Zhang and W. J. Wang, Synthesis of enriched oxygen vacancy TiO_2 microsphere with rapid response to isopropylamine and its application in herbicide detection, *Sens. Actuators, B*, 2022, **370**, 132423, DOI: 10.1016/j.snb.2022.132423.

25 D. Zhao, X. F. Zhang and W. J. Wang, Ultra-small TiO_2 nanocubes with highly active (001) facet for acetone fast detection and diagnosis of diabetes, *Microchem. J.*, 2023, **184**, 108122, DOI: 10.1016/j.microc.2022.108122.

26 Z. Li, A. A. Haidry, Y. S. Liu, L. C. Sun and L. J. Xie, Strongly coupled Ag/TiO_2 heterojunction: from one-step facile synthesis to effective and stable ethanol sensing performances, *J. Mater. Sci.: Mater. Electron.*, 2018, **29**, 19219–19227, DOI: 10.1007/s10854-018-0048-3.

27 X. Yang, H. Li, W. Zhang, M. X. Sun and L. Q. Li, High visible photo electrochemical activity of Ag nanoparticle-sandwiched CdS/Ag/ZnO nanorods, *ACS Appl. Mater. Interfaces*, 2017, **9**, 658–667, DOI: 10.1021/acsami.6b12259.

28 W. Kim, M. Choi and K. Yong, Generation of oxygen vacancies in ZnO nanorods/filmsand their effects on gas sensing properties, *Sens. Actuators, B*, 2015, **209**, 989–996, DOI: 10.1016/j.snb.2014.12.072.

29 X. W. Li, X. Zhou, H. Guo, C. Wang and J. Y. Liu, Design of Au@ZnO Yolk–Shell nanospheres with enhanced gas sensing properties, *ACS Appl. Mater. Interfaces*, 2014, **6**, 18661–18667, DOI: 10.1021/am5057322.